How Myopia and Glaucoma Influence the Biomechanical Susceptibility of the Optic Nerve Head

Thanadet Chuangsuwanich,[1,2] Tin A. Tun,[3,4] Fabian A. Braeu,[2,4] Clarice H. Y. Yeoh,[1] Rachel S. Chong,[4] Xiaofei Wang,[6] Tin Aung,[1,3,4] Quan V. Hoang,[1,3–5] and Michaël J. A. Girard[2,3,7]

[1]Yong Loo Lin School of Medicine, National University of Singapore, Singapore
[2]Ophthalmic Engineering & Innovation Laboratory, Singapore Eye Research Institute, Singapore National Eye Centre, Singapore
[3]Eye-ACP, Duke-NUS Medical School, Singapore, Singapore
[4]Singapore Eye Research Institute, Singapore National Eye Centre, Singapore, Singapore
[5]Department of Ophthalmology, Columbia University, New York, New York, United States
[6]Laboratory for Biomechanics and Mechanobiology of Ministry of Education, Beijing Advanced Innovation Center for Biomedical Engineering, School of Biological Science and Medical Engineering, School of Engineering Medicine, Beihang University, Beijing, China
[7]Institute for Molecular and Clinical Ophthalmology, Basel, Switzerland

Correspondence: Michaël J. A. Girard, Ophthalmic Engineering & Innovation Laboratory (OEIL), Singapore Eye Research Institute (SERI), The Academia, 20 College Road, Discovery Tower Level 6, Singapore, Singapore; mgirard@ophthalmic.engineering.
Quan V. Hoang, Singapore Eye Research Institute (SERI), The Academia, 20 College Road, Discovery Tower Level 6, Singapore, Singapore; donny.hoang@duke-nus.edu.sg.

Received: April 6, 2023
Accepted: July 6, 2023
Published: August 8, 2023

Citation: Chuangsuwanich T, Tun TA, Braeu FA, et al. How myopia and glaucoma influence the biomechanical susceptibility of the optic nerve head. *Invest Ophthalmol Vis Sci.* 2023;64(11):12. https://doi.org/10.1167/iovs.64.11.12

Purpose. The purpose of this study was to assess optic nerve head (ONH) deformations following acute intraocular pressure (IOP) elevations and horizontal eye movements in control eyes, highly myopic (HM) eyes, HM eyes with glaucoma (HMG), and eyes with pathologic myopia (PM) alone or PM with staphyloma (PM + S).

Methods. We studied 282 eyes, comprising of 99 controls (between +2.75 and −2.75 diopters), 51 HM (< −5 diopters), 35 HMG, 21 PM, and 75 PM + S eyes. For each eye, we imaged the ONH using spectral-domain optical coherence tomography (OCT) under the following conditions: (1) primary gaze, (2) 20 degrees adduction, (3) 20 degrees abduction, and (4) primary gaze with acute IOP elevation (to ∼35 mm Hg) achieved through ophthalmodynamometry. We then computed IOP- and gaze-induced ONH displacements and effective strains. Effective strains were compared across groups.

Results. Under IOP elevation, we found that HM eyes exhibited significantly lower strains (3.9 ± 2.4%) than PM eyes (6.9 ± 5.0%, $P < 0.001$), HMG eyes (4.7 ± 1.8%, $P = 0.04$), and PM + S eyes (7.0 ± 5.2%, $P < 0.001$). Under adduction, we found that HM eyes exhibited significantly lower strains (4.8% ± 2.7%) than PM + S eyes (6.0 ± 3.1%, $P = 0.02$). We also found that eyes with higher axial length were associated with higher strains.

Conclusions. Our study revealed that eyes with HMG experienced significantly greater strains under IOP compared to eyes with HM. Furthermore, eyes with PM + S had the highest strains on the ONH of all groups.

Keywords: optic nerve head (ONH), biomechanics, myopia, glaucoma, staphyloma

An association between glaucoma and myopia is well-established and has been reported in many clinical and population-based studies.[1–3] In myopia, the eye elongates and the posterior sclera remodels, thins, and weakens, resulting in a general loss of collagen and proteoglycans.[4–6] These changes can make the optic nerve head (ONH) more susceptible to biomechanical forces exerted by intraocular pressure (IOP), potentially causing damage to the axons at the lamina cribrosa (LC) and leading to the development of glaucoma.[7]

To date, providing an accurate diagnosis of glaucoma in patients with high myopia (HM) remains a major clinical challenge. This is because conventional biomarkers for glaucoma diagnosis, such as the appearance of the ONH, peripapillary atrophy (PP), and visual field (VF) defects on perimetry,[8,9] are often obscured by the structural changes typically found in HM, such as myopic PP atrophy, tilted disc, and thinning of the retinal nerve fiber layer (RNFL),[8,10] as well as in pathologic myopia (PM), such as geographic atrophic changes in myopic macular degeneration that result in VF defects.[11–13] With these limitations, a novel biomarker that can determine whether a given eye is glaucomatous, myopic, or a combination of both, would be clinically important.

In this study, we aimed to assess the biomechanics of the ONH under conditions of increased IOP and different horizontal gazes in patients with a range of myopia-related conditions, including HM, PM, pathologic myopia with staphyloma (PM + S), and those confirmed to have both high myopia and glaucoma (HMG). Our goal is to better understand how these conditions differ in terms of their sensitivity to external loads and to explore the potential of

using biomechanical tests to identify individuals with HM who are at risk of developing glaucoma.

Methods

Subjects Recruitment

We studied 282 eyes, which comprised of 99 controls, 51 HM, 35 HMG, 21 PM, and 75 PM + S from glaucoma clinics at the Singapore National Eye Centre. We included subjects aged more than 50 years old, of Chinese ethnicity (predominant in Singapore), and excluded subjects who underwent prior intraocular/orbital/brain surgeries, subjects with a medical history of strabismus, ocular trauma, ocular motor palsies, orbital/brain tumors; with clinically abnormal saccadic or pursuit eye movements; subjects with poor LC visibility in OCT (<50% en face visibility); subjects with known carotid or peripheral vascular disease; or with any other abnormal ocular conditions.

Control eyes had refractive error between +2.75 and −2.75 diopters with axial lengths less than 25 mm. Control eyes had normal IOP and no pathological features on the ONH and the retina. HM was defined by eyes with axial lengths greater than 25 mm and myopic refractive errors worse than 5 diopters. HMG was defined for eyes with both HM (excluding PM and staphyloma) and a glaucoma diagnosis as performed by a glaucoma specialist (authors R.S.C. and A.T.). PM (without staphyloma) was defined for eyes exhibiting both HM and myopic macular degeneration as defined by the meta-analysis for PM classification system,[14] or myopic traction maculopathy (without the presence of staphyloma). PM + S was defined as HM eyes with a clinical diagnosis of staphyloma based on multimodal imaging (fundus photography, optical coherence tomography (OCT), ultrasonography, and, in selected subjects, magnetic resonance imaging) and confirmed by a retinal specialist.

Glaucoma was defined as glaucomatous optic neuropathy (based on Nagaoka et al., 2015),[15] characterized as loss of neuroretinal rim with vertical cup-to-disc ratio >0.7 or focal notching with nerve fiber layer defect attributable to glaucoma (based on a clinical observation) and/or asymmetry of cup-to-disc ratio between eyes >0.2, with repeatable glaucomatous visual field defects (independent of the IOP value) in at least one eye.

Each subject underwent the following ocular examinations: (1) measurement of refraction using an autokeratometer (RK-5; Canon, Tokyo, Japan) and (2) measurement of axial length, central corneal thickness, and anterior chamber depth using a commercial device (Lenstar LS 900; Haag-Streit AG, Switzerland). For each tested eye, we performed a visual field test using a standard achromatic perimetry with the Humphrey Field Analyser (Carl Zeiss Meditec, Dublin, CA, USA).

This study was approved by the SingHealth Centralized Institutional Review Board and adhered to the tenets of the Declaration of Helsinki. Written informed consent was obtained from each subject.

OCT Imaging

Subjects' pupils were dilated with 1.0% Tropicamide before imaging with spectral-domain OCT (Spectralis; Heidelberg Engineering GmbH, Heidelberg, Germany). The imaging protocol was similar to that from our previous work.[16] We conducted a raster scan of the ONH (covering a rectangular region of 15 degrees × 10 degrees centered at the ONH), comprising of 97 serial B-scans, with each B-scan comprising of 384 A-scans (Fig. 1a). The average distance between B-scans was 35.1 µm and the axial and lateral B-scan pixel resolution were, on average, 3.87 µm and 11.5 µm, respectively. All B-scans were averaged 20 times during acquisition to reduce speckle noise. Each eye was scanned 4 times under 4 different conditions – primary OCT position, 20 degrees adduction, 20 degrees abduction, and acute IOP elevation.

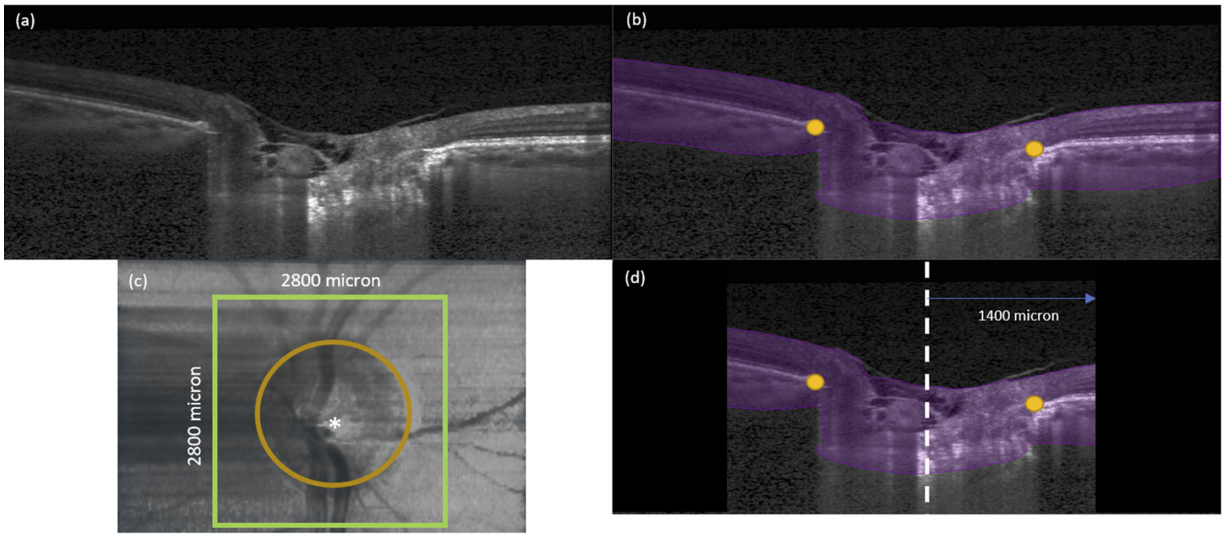

Figure 1. (**a**) A single B-scan obtained from the OCT machine without any image enhancement. (**b**) Automatic segmentation of the B-scan in (**a**). ONH tissues were segmented in *purple*. In addition, BMOs (*orange dots*) were automatically marked for each B-scan. (**c**) Anterior-surface view of the ONH. The ONH center (*white star*) was identified from the best-fit circle to the BMOs (*orange dotted line*). The *green square* defines our region of interest to be cropped from the OCT volume with 2800 µm length on each side. (**d**) A B-scan view after we apply cropping to the OCT volumes. The *black region* was not considered for our deformation tracking. The length from central line (*white dotted line*) to the cropping border (*green line*) is 1400 µm.

Investigative Ophthalmology & Visual Science

OCT Imaging in Primary Gaze and in Adduction/Abduction Positions

In this study, the primary gaze OCT position referred to the eye position during a standard OCT scan. This position may differ significantly from the true primary gaze position of 0 degrees because both the pupil and ONH need to be aligned with the OCT objective, which can cause an eye rotation to the left in a right eye, and vice versa.[16] In our previous study,[17] we estimated the angle to be approximately 7 degrees. This estimation was derived using a geometric method that involved multiple subjects fixating on a target positioned 2 meters away from the OCT machine, utilizing their non-imaged eye. By laterally adjusting the position of the fixation target until the fovea became visible on the OCT image, we determined the angular distance between the ONH and the fovea, referred to as the offset angle. Notably, prior investigations conducted by Demer et al.[18] and Suh et al.[19] reported an approximate angle of 12 degrees. Thus, our horizontal eye movement of 20 degrees in either direction was with respect to the OCT reference configuration.

Procedures for imaging under different gaze positions have been described in our previous work.[16] Briefly, we used a custom-built 3D printed rotatable chin rest to induce 20 degrees adduction and 20 degrees abduction, and one OCT volume was acquired in each position.

OCT Imaging During Acute IOP Elevation

For each eye in the primary gaze position, we applied a constant force of 0.65 N to the temporal side of the lower eyelid using an ophthalmodynamometer (ODM), as per an established protocol.[16,20,21] The force was consistently applied via ODM throughout the entire duration of the OCT scan, which ranged from 2 to 3 minutes for each subject. This force raised IOP to about 35 mm Hg and was maintained constant. IOP was then re-assessed with a Tono-Pen (Reichert Instruments GmbH, Munich, Germany), and the ONH was imaged with OCT in baseline position immediately (within 30 seconds) after the IOP was measured.

In Vivo Displacement and Strain Mapping of the ONH

For every OCT volume, we used an automated process to segment the ONH (Fig. 1b). This segmentation involved identifying the anterior boundary, represented by the inner limiting membrane, as well as discerning the visible posterior boundary, which encompasses the visible portion of the posterior sclera, choroid, and the LC. The segmentation algorithm was trained to delineate the whole ONH region using images from patients with glaucoma and healthy individuals. The segmentation algorithm's architecture was similar to that of our previous publications, albeit with slight modifications aimed at segmenting the entire ONH tissue, rather than distinguishing between different tissues.[21,22] We used a commercial DVC module (Amira, 2020.3; Thermo Fisher Scientific, Waltham, MA, USA) to map the three-dimensional deformations between the baseline scan and scans under external loads (adduction, abduction, or elevated IOP) for each patient. The DVC algorithm was used in our previous study to study associations between biomechanical strain and visual field loss.[21] Details of the DVC algorithm used in this study, including how the strain values are derived and the validation of our DVC algorithm were provided in our previous paper and in the Supplemental Appendix SA.[21]

For each OCT volume, IOP- and gaze-induced effective strains were averaged across the entire ONH region within a 2800 × 2800 µm en face region centered on the Bruch's membrane opening (BMO) center (see Fig. 1).

Because there were variations in the level of IOP increase across subjects (IOP under ODM minus baseline IOP), due to the variations in tissue properties and eye geometry among subjects, we would like to adjust the measured effective strain accordingly. Comparing these resulting strains without normalization would introduce bias, as each individual ONH experiences different IOP loads despite the application of a constant force. To achieve this, we multiplied the measured effective strain by the ratio between the average level of IOP increase observed across all subjects (18 mm Hg) and the individual IOP increase (elevated IOP minus baseline IOP) according to Equation 1.

$$Adjusted\ Effective\ Strains = Measured\ Effective\ Strain \times \frac{18\ (mmHg)}{Elevated\ IOP\ (mmHG) - Baseline\ IOP\ (mmHg)} \quad (1)$$

Whereas our equation holds true under the assumption of a linear relationship between stress and strain, we acknowledged the presence of nonlinear behaviors in load-bearing soft connective tissues of the eye, such as the sclera, lamina, and Bruch's membrane. Nonetheless, research studies conducted by Fazio et al.[23] and Grytz et al.[24] on human scleral strains, as well as by Midgett et al.[25] on human LC strains, have revealed that beyond the 18 mm Hg threshold (the baseline IOP of our patients), the effects of nonlinearity diminish. To further validate our normalization approach, we computed the errors in strain that could have arisen from such nonlinear behaviors. Errors were estimated using the IOP versus strain curves for the aforementioned three references, and using our own IOP ranges. We found that the error in strain (due to a linear assumption) was considerably small, and could be estimated by a normal distribution (mean = 0.09%, STD = 0.13%).

Statistical Analysis

Statistical analyses were performed using MATLAB (version 2018a; The MathWorks, Inc., Natick, MA, USA). Effective strains were subjected to statistical analysis as continuous variables, which represent numeric values with an infinite number of possible values between any two given values. To perform statistical analysis, we split our investigation into (1) differences in strains between HM and HMG under each load and (2) differences in strains among myopia spectrum (HM, PM, and PM + S) under each load. We used independent samples *t*-test (MATLAB function – *t*-test2) to compare the mean values of effective strain between the diagnostic groups. Analysis of variance (MATLAB function - ANOVA) was used to determine the differences across groups in age, axial length, visual field mean deviation (MD), pattern standard deviation (PSD), and IOP on the day of the experiment. Linear regressions were used to study the associations between (1) axial length (or refractive error) and ONH effective strains; and those between (2) adduction-induced strains and IOP-induced strains. Statistical significance level was set at 0.05.

Results

Demographics

We excluded 6 subjects with HM, 5 subjects with HMG, 5 subjects with PM, and 11 subjects with PM + S from the study due to poor en face LC visibility (<50% of the BMO area), and therefore 99 controls, 45 subjects with HM, 30 subjects with HMG, 16 subjects with PM, and 64 subjects with PM + S were included in the final analysis.

There were significant differences ($P < 0.05$) in terms of age, axial length, and visual field (MD and PSD values) between groups (see the Table). Notably, subjects with HM were on average younger as compared to other groups. Subjects with myopia (HM, HMG, PM, and PM + S) exhibited a higher axial length as compared to the control group. Subjects with HMG, PM, and PM + S had poorer visual field indices (a more negative MD and a more positive PSD) as compared to the HM and control groups. There was no

Table. Characteristics of Eyes in Each Group

	Mean ± Standard Deviation or *n* (%)				
Characteristic	**Control**	**HM**	**HMG**	**PM**	**PM + S**
Age, y	64 ± 7	57 ± 5	62 ± 8	60 ± 9	63 ± 7
Sex, F, %	51	53	30	31	44
Axial length, mm	24.0 ± 1.0	26.8 ± 1.0	27.1 ± 1.0	29.1 ± 2.2	31 ± 2.3
Visual filed, MD, dB	−0.9 ± 1.8	−1.27 ± 3.0	−8.0 ± 6.5	−5.7 ± 4.6	−10.4 ± 7.1
Pattern standard deviation, dB	2.0 ± 1.1	2.18 ± 1.2	7.4 ± 4.5	5.1 ± 2.75	6.6 ± 2.82
IOP on the day of the experiment (mm Hg)*	15.5 ± 2.7	15.6 ± 2.3	15.7 ± 2.3	15.8 ± 2.8	17.2 ± 3.3

* This is IOP after treatment for subjects with HMG.

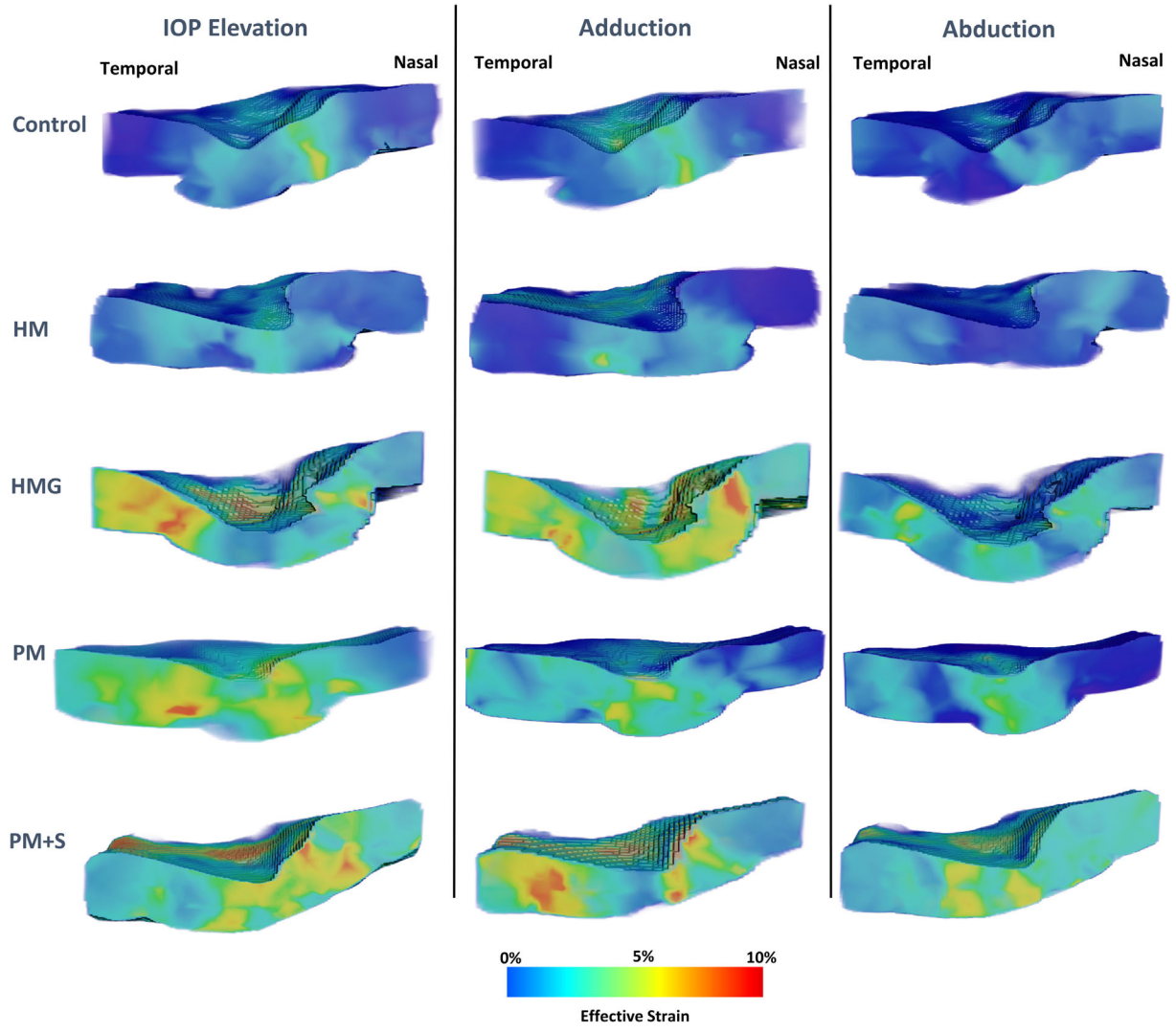

Figure 2. Three-dimensional effective strain maps of a sample eye (with central cut through the ONH) for each diagnostic group under loads.

Investigative Ophthalmology & Visual Science

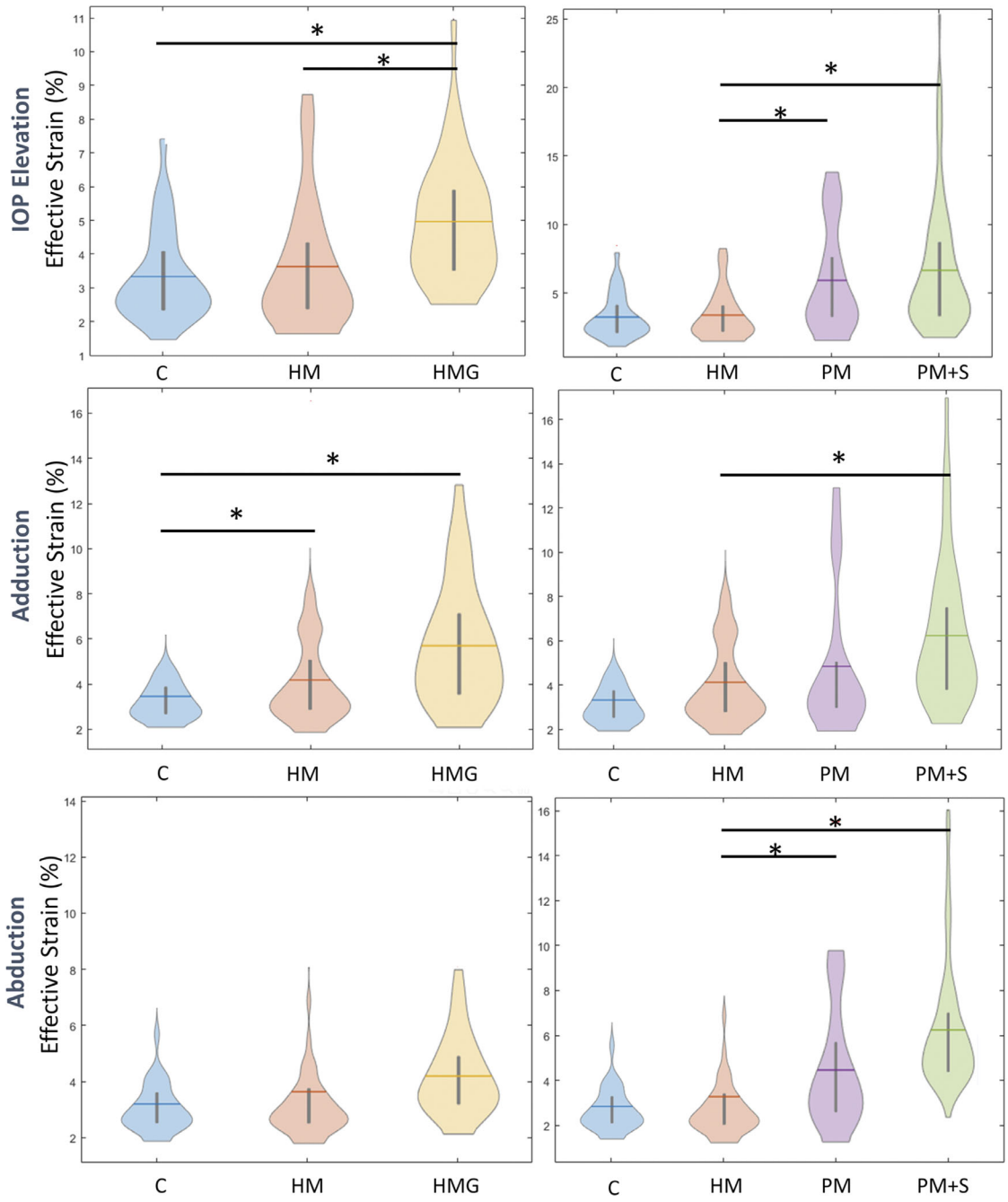

Figure 3. Violin-plot showing average ONH effective strains for each group under IOP elevation, Adduction and abduction. The *left column* represents a comparison between HM and HMG and the *right column* represents a comparison across the myopia spectrum. * Denotes significant differences between the two groups.

significant difference in presenting IOP on the day of experiment between groups.

IOP-Induced ONH Strains

A visualization of strain maps (one eye from each diagnostic group) was given in Figure 2. Controls exhibited the least IOP-induced strains (3.6 ± 1.6%), followed by HM (3.9 ± 2.4%), HMG (4.7 ± 1.8%), PM (6.9 ± 5.0%), and PM + S (7.0 ± 5.2%).

We found that HM eyes exhibited significantly lower strains under IOP elevation than PM eyes ($P < 0.001$), HMG eyes ($P = 0.04$), and PM + S eyes ($P < 0.001$; Fig. 3). There was no significant difference in IOP-induced strains between control and HM eyes.

Gaze-Induced ONH Strains

Under abduction, we found a similar trend as that observed with IOP, with controls exhibiting the least strains

Investigative Ophthalmology & Visual Science

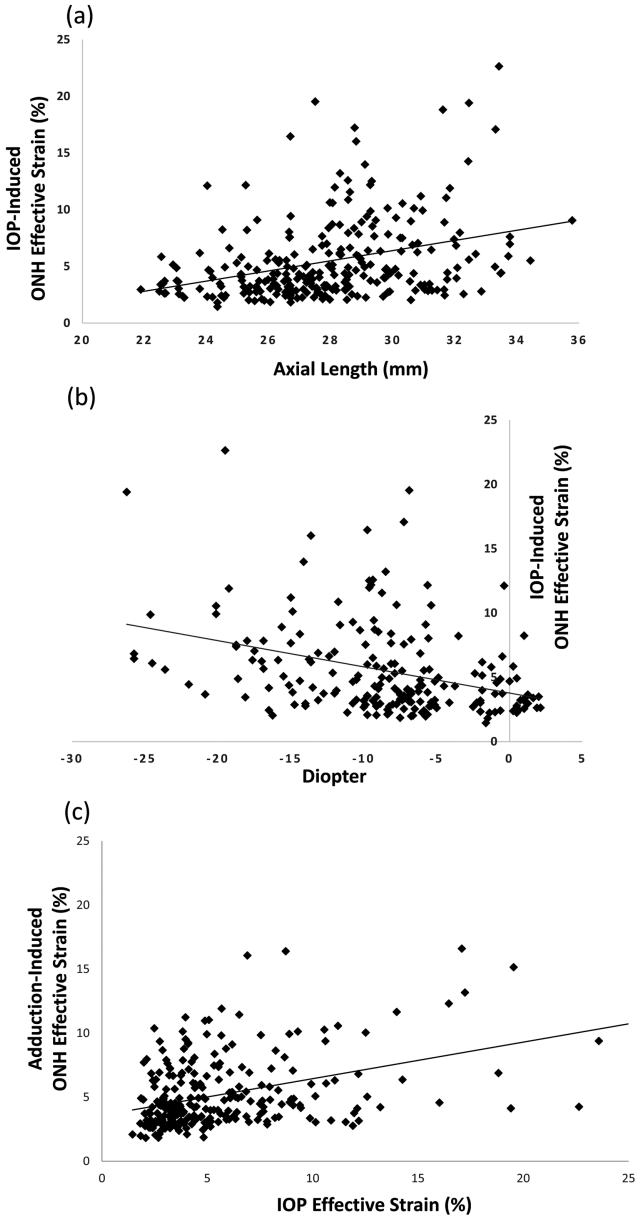

Figure 4. Scatterplot showing a significant linear relationship between ONH effective strain under IOP elevation and (**a**) axial length (mm) and (**b**) refractive error of all eyes. (**c**) Scatterplot showing a significant positive linear relationship between ONH effective strain under IOP elevation and adduction.

(3.3 ± 1.4%), followed by HM (3.9 ± 2.4%), HMG (4.1 ± 1.4%), PM (5.0 ± 2.5%), and PM + S (5.3 ± 3.0%). Additionally, we found that PM + S eyes exhibited significantly higher strains than HM ($P < 0.05$) and PM eyes exhibited significantly higher strains than HM ($P < 0.05$) under abduction. We found no significant difference in abduction-induced strain between subjects with HM and controls.

Under adduction, we found that controls exhibited the least strains (3.8 ± 1.6%), followed by HM (4.8 ± 2.7%), PM (5.2 ± 2.5%), HMG (5.7 ± 2.5%), and PM + S (6.0 ± 3.1%). Additionally, we found that HM eyes exhibited significantly higher strain than controls ($P < 0.05$) and PM + S eyes exhibited significantly higher strain than HM eyes ($P < 0.05$; see Fig. 3).

Overall, Large ONH Strains (IOP-Induced) Were Associated With High Axial Length or Low Refractive Error

Across all eyes, we found that the eyes that exhibited the largest IOP-induced ONH strains were also the eyes that had a higher axial length ($P < 0.001$, an axial length increase of approximately 2 mm results in an 1% increase in ONH strain) or a more negative refractive error ($P < 0.001$, a worsening diopter of approximately 1 unit results in an 1% increase in ONH strain; Figs. 4a, 4b).

Adduction-Induced ONH Strains Were Associated With IOP-Induced Strains

Across all eyes, we found that adduction-induced ONH strains were positively associated with IOP-induced strains ($P < 0.001$; Fig. 4c).

Discussion

We found that control eyes exhibited the lowest strains under increased IOP, followed by HM, HMG, PM, and PM + S. This trend was also observed during horizontal gaze, and we found that strains induced by IOP and gaze were correlated. Overall, the eyes with the most severe conditions (PM + S) exhibited the highest strains under all conditions, reaching 7% under IOP elevation. Our findings suggest that there are significant differences in strain response (under acute IOP elevation) between eyes with HMG and eyes with HM, hinting at the possibility of using simple biomechanical tests to identify myopic eyes that have underlying glaucoma.

We found that the ONH of HMG eyes exhibited higher levels of IOP-induced strain as compared to HM eyes. This may be explained by ONH excavation and deformation of the LC, a load bearing structure of the ONH, such as its thinning and posterior bowing in glaucoma.[26–30] Jonas et al.[31] found that among HM eyes, the presence of glaucoma was associated with thinner LC than in non-highly myopic eyes, which would promote a more structurally compliant response and thus greater strain.[32,33] It is possible that the compounded effect of myopia (scleral thinning,[34,35] tissue loss,[35] and increase in small diameter collagen fibrils[35]) and glaucoma that results in greater strain in HMG eyes compared to HM eyes. Another potential factor maybe shifts in central retinal vessel trunks (CRVTs), during axial length elongation[36] and glaucoma development,[37] which could contribute to the greater structural weakening of HMG eyes.[38,39] Our results suggest that HMG eyes may have a different biomechanical sensitivity than HM eyes as revealed by a simple biomechanical test. Future studies should aim to unravel the combined biomechanical influences of tissue remodeling associated with the development of glaucoma and myopia in terms of quantifiable strains.

We observed that eyes with PM, especially those with staphylomas, exhibited significantly higher strains than eyes with HM under all loads. PM, especially with the presence of staphylomas, is often associated with myopic traction maculopathy and both conditions are known to be responsible for structural weakening of the ocular globe.[40] Posterior staphylomas are associated with thinning and elongation of the local sclera and deformity of the posterior ocular segment.[41] Norman et al.[42] showed that a thinner posterior sclera deformed more easily, and that scleral canal

expansion and LC deformation would be larger than that seen with a thicker sclera. PM eyes are also associated with an extreme increase in axial length and further structural weakening of the sclera.[43] We also suspect that a proportion of our subjects with PM would go on to develop staphylomas, and we aim to monitor this closely.

We found that the ONH of eyes with HM exhibited higher strain than that in controls eyes under adduction. Under adduction, the optic nerve sheath has been observed to exert significant tractional forces on the ONH which caused the ONH to deform in a distinct "see-saw" pattern.[18,21,44–46] Our findings indicate that HM eyes were more susceptible to this tractional force as compared to control eyes, which is expected due to the weakening of the sclera during myopia development.[47] Under IOP elevation, we found that both subjects with HM and the controls exhibited the same level of strains, which was an unexpected finding as we had expected that the HM eyes would also be more sensitive to IOP elevation than the controls. According to a review by Boote C. et al.,[48] there have been no studies that investigated the in vivo IOP-induced ONH strains between subject groups with different myopic status, thus we cannot compare our findings directly with pre-existing results. This nonsignificant finding under IOP elevation could be due to our relatively small number of subjects in the HM groups (51 subjects), and the fact that we used a binary division (25 mm in axial length) to separate non-HM from HM, several subjects in both groups had an axial length that were close to 25 mm. These subjects could affect the observed trends given our number of subjects with HM. In a future study, we plan to recruit more subjects with HM to better understand this trend.

We also found a strong association between axial length and ONH strains under all loads, as well as between refractive error and ONH strains under all loads. Our findings indicated a distinct weakening of the sclera across a spectrum of myopia severity, as defined by axial length. Axial length is also a risk factor in glaucoma[49,50] and the link between the two factors maybe biomechanical. A longitudinal study that captures the ONH morphological changes and pathological changes in myopic group across a spectrum of axial length would be of importance to establish this relationship more strongly.

Several limitations in this study require further discussion. First, OCT imaging did not capture the full thickness of the sclera in all eyes, limiting the representativeness of our strains for the posterior peripapillary sclera. Moreover, delineating the boundaries of LC tissue in PM eyes proved challenging due to their atypical morphology. This hampers accurate segmentation of LC tissues and restricts the comparison of LC strains across subject groups. Nonetheless, we quantified average strains of all ONH tissues within each sector, as detailed in Appendix B. Our findings reveal higher average effective strains in the nasal region compared to the temporal region, and higher average effective strains in the central region as compared to the peripheral region. However, establishing a more robust correlation between regional LC strains and visual field loss in HM eyes requires and improvement in OCT image quality or adapting segmentation tools for PM cases. Addressing these limitations will enhance our understanding of the relationship between LC strains and visual field abnormalities in highly myopic eyes.

Second, the use of ODM could introduce experimental errors as we applied an external force to the anterior sclera through the eyelid. We could not directly control the stress experienced at the ONH across subjects, and there may be variations due to the outflow facility[51] and the biomechanical characteristics[52] of each eye. Additionally, IOP also fluctuates during the scan duration due to the presence of the ocular pulse.[53] The actual level of IOP raised via ODM could also potentially decline during the time needed for the OCT acquisition.[54] Such a decline may also vary across subjects depending on the outflow facility[51] and the biomechanical characteristics[52] of each eye. Thus, this constituted another uncontrolled variable in our study.

Last, our subjects with HM were relatively younger compared to the controls; however, we believe that this would not significantly affect our result because our subjects were from an older population (more than 50 years of age) and notable changes in scleral elastin fibers and extracellular matrix should have occurred at an earlier age.[48]

We proposed a simple test to map 3D ONH strains in a clinical setting, which could potentially be used to distinguish between eyes with HMG and eyes with HM alone. Given the strong correlation between IOP-induced strains and adduction induced strains, a noninvasive test using adduction to induce a biomechanical response is particularly attractive, as it requires no direct force application to the patient's eye. In the future, we also aim to approximate the level of stress and material properties of the ocular tissues from the measured displacement fields, utilizing techniques such as the virtual field method.[55] This approach will provide a more complete picture of the biomechanical status of the eye.

Acknowledgments

The authors thank the (1) the donors of the National Glaucoma Research, a program of the BrightFocus Foundation, for support of this research (G2021010S [MG]), (2) the NMRC-LCG grant "TAckling & Reducing Glaucoma Blindness with Emerging Technologies (TARGET)," award ID: MOH-OFLCG21jun-0003 [MJAG] (3) the "Retinal Analytics through Machine learning aiding Physics (RAMP)" project supported by the National Research Foundation, Prime Minister's Office, Singapore under its Intra-Create Thematic Grant "Intersection of Engineering and Health" - NRF2019-THE002-0006 awarded to the Singapore MIT Alliance for Research and Technology (SMART) Centre, (4) SingHealth DukeNUS, Academic medicine research grant (AM/SU053/2021 [TAT]) (5) the National Natural Science Foundation of China (12002025 [XW]) and (6) the NMRC Clinician Scientist Award grant, award ID: MOH-CSAINV18may-0003 [QVH].

Disclosure: **T. Chuangsuwanich**, None; **T.A. Tun**, None; **F.A. Braeu**, None; **C.H.Y. Yeoh**, None; **R.S. Chong**, None; **X. Wang**, None; **T. Aung**, None; **Q.V. Hoang**, None; **M.J.A. Girard**, is the co-founder of the AI start-up company Abyss Processing Pte Ltd.

References

1. Shen L, Melles RB, Metlapally R, et al. The association of refractive error with glaucoma in a multiethnic population. *Ophthalmology*. 2016;123(1):92–101.
2. Perera SA, Wong TY, Tay W-T, et al. Refractive error, axial dimensions, and primary open-angle glaucoma: the Singapore Malay Eye Study. *Arch Ophthalmol*. 2010;128(7):900–905.
3. Grødum K, Heijl A, Bengtsson B. Refractive error and glaucoma. *Acta Ophthalmol Scand*. 2001;79(6):560–566.
4. McBrien NA, Jobling AI, Gentle A. Biomechanics of the sclera in myopia: extracellular and cellular factors. *Optometry and Vision Sci*. 2009;86(1):E23–E30.

5. McBrien NA, Gentle A. Role of the sclera in the development and pathological complications of myopia. *Prog Retin Eye Res*. 2003;22(3):307–338.
6. Levy AM, Fazio MA, Grytz R. Experimental myopia increases and scleral crosslinking using genipin inhibits cyclic softening in the tree shrew sclera. *Ophthalmic Physiol Opt*. 2018;38(3):246–256.
7. Grytz R, Yang H, Hua Y, et al. Connective tissue remodeling in myopia and its potential role in increasing risk of glaucoma. *Curr Opinion Biomedical Engineer*. 2020;15:40–50.
8. Chang RT, Singh K. Myopia and glaucoma: diagnostic and therapeutic challenges. *Curr Opinion in Ophthalmol*. 2013;24(2):96–101.
9. Shin H-Y, Park H-YL, Park CK. The effect of myopic optic disc tilt on measurement of spectral-domain optical coherence tomography parameters. *Br J Ophthalmol*. 2015;99(1):69–74.
10. Hwang YH, Kim YY, Jin S, et al. Errors in neuroretinal rim measurement by Cirrus high-definition optical coherence tomography in myopic eyes. *Br J Ophthalmol*. 2012;96(11):1386–1390.
11. Ohno-Matsui K, Shimada N, Yasuzumi K, et al. Long-term development of significant visual field defects in highly myopic eyes. *Am J Ophthalmol*. 2011;152(2):256–265.e1.
12. Holden BA, Fricke TR, Wilson DA, et al. Global prevalence of myopia and high myopia and temporal trends from 2000 through 2050. *Ophthalmology*. 2016;123(5):1036–1042.
13. Marcus MW, de Vries MM, Montolio FGJ, Jansonius NM. Myopia as a risk factor for open-angle glaucoma: a systematic review and meta-analysis. *Ophthalmology*. 2011;118(10):1989–1094.e2.
14. Ohno-Matsui K, Kawasaki R, Jonas JB, et al. International photographic classification and grading system for myopic maculopathy. *Am J Ophthalmol*. 2015;159(5):877–883.e7.
15. Nagaoka N, Jonas JB, Morohoshi K, et al. Glaucomatous-type optic discs in high myopia. *PLoS One*. 2015;10(10):e0138825.
16. Wang X, Beotra MR, Tun TA, et al. In vivo 3-dimensional strain mapping confirms large optic nerve head deformations following horizontal eye movements. *Invest Ophthalmol Vis Sci*. 2016;57(13):5825–5833.
17. Fisher LK, Wang X, Tun TA, et al. Gaze-evoked deformations of the optic nerve head in thyroid eye disease. *Br J Ophthalmol*. 2021;105(12):1758–1764.
18. Demer JL, Clark RA, Suh SY, et al. Optic nerve traction during adduction in open angle glaucoma with normal versus elevated intraocular pressure. *Curr Eye Res*. 2020;45(2):199–210.
19. Suh SY, Le A, Shin A, et al. Progressive deformation of the optic nerve head and peripapillary structures by graded horizontal duction. *Invest Ophthalmol Vis Sci*. 2017;58(12):5015–5021.
20. Beotra MR, Wang X, Tun TA, et al. In vivo three-dimensional lamina cribrosa strains in healthy, ocular hypertensive, and glaucoma eyes following acute intraocular pressure elevation. *Invest Ophthalmol Vis Sci*. 2018;59(1):260–272.
21. Chuangsuwanich T, Tun TA, Braeu FA, et al. Differing associations between optic nerve head strains and visual field loss in normal-and high-tension glaucoma subjects. *Ophthalmology*. 2023;130(1):99–110.
22. Devalla SK, Renukanand PK, Sreedhar BK, et al. DRUNET: a dilated-residual U-Net deep learning network to segment optic nerve head tissues in optical coherence tomography images. *Biomedical Optics Express*. 2018;9(7):3244–3265.
23. Fazio MA, Grytz R, Morris JS, et al. Age-related changes in the non-linear mechanical strain response of human peripapillary sclera. *Summer Bioengineering Conference: American Society of Mechanical Engineers*. 2013; vol. 55614.
24. Grytz R, Fazio M, Libertiaux V, et al. Racial differences in human scleral material properties. *Invest Ophthalmol Vis Sci*. 2013;54(15):79.
25. Midgett DE, Jefferys JL, Quigley HA, Nguyen TD. The inflation response of the human lamina cribrosa and sclera: analysis of deformation and interaction. *Acta Biomater*. 2020;106:225–241.
26. Quigley HA, Varma R, Tielsch JM, et al. The relationship between optic disc area and open-angle glaucoma: the Baltimore Eye Survey. *J of Glaucoma*. 1999;8(6):347–352.
27. Quigley HA, Addicks EM, Green WR, Maumenee A. Optic nerve damage in human glaucoma: II. The site of injury and susceptibility to damage. *Arch Ophthalmol*. 1981;99(4):635–649.
28. Kwon YH, Fingert JH, Kuehn MH, Alward WL. Primary open-angle glaucoma. *N Engl J Med*. 2009;360(11):1113–1124.
29. Yang H, Downs JC, Bellezza A, et al. 3-D histomorphometry of the normal and early glaucomatous monkey optic nerve head: prelaminar neural tissues and cupping. *Invest Ophthalmol Vis Sci*. 2007;48(11):5068–5084.
30. Bellezza AJ, Rintalan CJ, Thompson HW, et al. Deformation of the lamina cribrosa and anterior scleral canal wall in early experimental glaucoma. *Invest Ophthalmol Vis Sci*. 2003;44(2):623–637.
31. Jonas JB, Berenshtein E, Holbach L. Lamina cribrosa thickness and spatial relationships between intraocular space and cerebrospinal fluid space in highly myopic eyes. *Invest Ophthalmol Vis Sci*. 2004;45(8):2660–2665.
32. Sigal I, Yang H, Roberts M, et al. The effect of lamina cribrosa thickness and position on optic nerve head biomechanics. *Invest Ophthalmol Vis Sci*. 2008;49(13):3668.
33. Midgett D, Liu B, Ling YTT, et al. The effects of glaucoma on the pressure-induced strain response of the human lamina cribrosa. *Invest Ophthalmol Vis Sci*. 2020;61(4):41.
34. Phillips J, McBrien N. Form deprivation myopia: elastic properties of sclera. *Ophthalmic Physiol Opt*. 1995;15(5):357–362.
35. McBrien NA, Cornell LM, Gentle A. Structural and ultrastructural changes to the sclera in a mammalian model of high myopia. *Invest Ophthalmol Vis Sci*. 2001;42(10):2179–2187.
36. Lee KM, Choung H-K, Kim M, et al. Positional change of optic nerve head vasculature during axial elongation as evidence of lamina cribrosa shifting: Boramae Myopia Cohort Study Report 2. *Ophthalmology*. 2018;125(8):1224–1233.
37. Panda SK, Cheong H, Tun TA, et al. The three-dimensional structural configuration of the central retinal vessel trunk and branches as a glaucoma biomarker. *Am J Ophthalmol*. 2022;240:205–216.
38. Wang B, Lucy KA, Schuman JS, et al. Location of the central retinal vessel trunk in the laminar and prelaminar tissue of healthy and glaucomatous eyes. *Sci Rep*. 2017;7(1):1–6.
39. Jonas JB, Budde WM, Németh J, et al. Central retinal vessel trunk exit and location of glaucomatous parapapillary atrophy in glaucoma. *Ophthalmology*. 2001;108(6):1059–1064.
40. Jonas JB, Ohno-Matsui K, Holbach L, Panda-Jonas S. Histology of myopic scleral staphylomas. *Invest Ophthalmol Vis Sci*. 2019;60(9):4354.
41. Maruko I, Iida T, Sugano Y, et al. Morphologic analysis in pathologic myopia using high-penetration optical coherence tomography. *Invest Ophthalmol Vis Sci*. 2012;53(7):3834–3838.
42. Norman RE, Flanagan JG, Sigal IA, et al. Finite element modeling of the human sclera: influence on optic nerve head biomechanics and connections with glaucoma. *Exp Eye Res*. 2011;93(1):4–12.
43. Saka N, Ohno-Matsui K, Shimada N, et al. Long-term changes in axial length in adult eyes with pathologic myopia. *Am J Ophthalmol*. 2010;150(4):562–568.e1.

Investigative Ophthalmology & Visual Science

44. Sibony PA, Wei J, Sigal IA. Gaze-evoked deformations in optic nerve head drusen: repetitive shearing as a potential factor in the visual and vascular complications. *Ophthalmology*. 2018;125(6):929–937.
45. Wang X, Rumpel H, Lim WEH, et al. Finite element analysis predicts large optic nerve head strains during horizontal eye movements. *Invest Ophthalmol Vis Sci*. 2016;57(6):2452–2462.
46. Sibony PA. Gaze evoked deformations of the peripapillary retina in papilledema and ischemic optic neuropathy. *Invest Ophthalmol Vis Sci*. 2016;57(11):4979–4987.
47. Wang X, Chang S, Grinband J, et al. Optic nerve tortuosity and displacements during horizontal eye movements in healthy and highly myopic subjects. *Br J Ophthalmol*. 2022;106(11):1596–1602.
48. Boote C, Sigal IA, Grytz R, et al. Scleral structure and biomechanics. *Prog Retin Eye Res*. 2020;74:100773.
49. Oku Y, Oku H, Park M, et al. Long axial length as risk factor for normal tension glaucoma. *Graefe's Arch for Clinic Exp Ophthalmol*. 2009;247(6):781–787.
50. Jonas JB, Weber P, Nagaoka N, Ohno-Matsui K. Glaucoma in high myopia and parapapillary delta zone. *PLoS One*. 2017;12(4):e0175120.
51. Kazemi A, McLaren JW, Lin S-C, et al. Comparison of aqueous outflow facility measurement by pneumatonography and digital Schiøtz tonography. *Invest Ophthalmol Vis Sci*. 2017;58(1):204–210.
52. Grytz R, Fazio MA, Girard MJ, et al. Material properties of the posterior human sclera. *J Mech Behav Biomed Mater*. 2014;29:602–617.
53. Dastiridou AI, Ginis HS, De Brouwere D, et al. Ocular rigidity, ocular pulse amplitude, and pulsatile ocular blood flow: the effect of intraocular pressure. *Invest Ophthalmol Vis Sci*. 2009;50(12):5718–5722.
54. Kronfeld PC. Tonography. *AMA Arch of Ophthalmol*. 1952;48(4):393–404.
55. Zhang L, Thakku SG, Beotra MR, et al. Verification of a virtual fields method to extract the mechanical properties of human optic nerve head tissues in vivo. *Biomech Model Mechanobiol*. 2017;16(3):871–887.

Investigative Ophthalmology & Visual Science